Wiley Analytical Science

Specific Heat Capacity Determination by DSC

April 19, 10:00am - 11:00am EDT

Specific heat capacity (cp) is an important, temperature-dependent material property and is often specified in material data sheets. It is a key property for improving technical processes such as injection molding, spray drying, or crystallization, as well as for the safety analysis of chemical processes and the design of chemical reactors.

Watch this session during the WAS Virtual Conference:

Dr. Jürgen Schawe

Register Now

This talk is sponsored by METTLER TOLEDO

ADVANCED FUNCTIONAL MATERIALS
www.afm-journal.de

Chiral Metallopolymers for Redox-Mediated Enantioselective Interactions

*Jemin Jeon, Johannes Elbert, Ching-Hsiu Chung, Junice Chae, and Xiao Su**

Synthetic chiral platforms can be a powerful platform for enantioselective interactions, especially when coupled with redox-mediated electrochemical processes. While metallopolymers are versatile platforms for molecularly selective binding, their application for chiral applications is limited. In particular, the recognition and separation of biologically relevant chiral molecules can be key for biomanufacturing and diagnostics. Here, the design of chiral redox-polymers enables electrochemically-controlled enantioselective interactions, and supramolecular chirality is leveraged for enhancing recognition towards target enantiomers. Chiral redox-metallopolymers are synthesized based on Ugi's amine-inspired chiral monomers, and their enantioselective recognition toward ionic enantiomers such as tryptophan and naproxen is demonstrated, with higher enanhcement provided by the chiral redox-polymer over the single-site, chiral building bloack itelf. 2D nuclear magnetic resonance spectroscopy and solid-state circular dichroism support the emergence of supramolecular chirality resulting from the intramolecular interaction between the ferrocene and the alkyl group in the backbone. The half potential shift of the redox-polymers behaves linearly from 0% to 100%ee L-tryptophan to enable enantiomer quantification. Investigation on solvent polarity and pH effect reveal that the enantioselective mechanism is attributed to the subtle balance between hydrogen bonding and π–π interaction. This study highlights the potential of chiral redox-metallopolymers as platforms for electrochemically-modulated enantioselective interactions towards a range of amino acids and pharmaceutical carboxylates.

1. Introduction

Enantioselective interactions are key to molecular diagnostics,[1] chiral purification,[2] asymmetric catalysis,[3,4] and a central feature of enzymatic processes.[5] The design of heterogeneous platforms for enantioselective recognition, especially through stimuli-responsive interfaces, can provide a powerful platform for chiral-based applications. Redox metallopolymers represent a distinct class of versatile functional materials and have been extensively studied for a wide scope of applications such as membranes,[6] self-assembly,[7] hydrogels,[8] and redox-mediated ion separation.[9] However, many of these studies have focused on achiralbinding and release of molecules, with limited studies on chirality strategies for enantioselective interactions. Therefore, we design a new chiral redox-polymer with chiral ferrocene (Fc) building blocks, that can serve as an electro-responsive enantioselective platform.

Fc derivatives have been used as an electron-transport mediators,[10] or as chiral selector in the homogeneous phase.[11] However, these homogeneous systems have often suffered from insufficient selectivity, the recovery of the sensor molecule, a lack of systematic signal quantification, and solubility limitations. Heterogeneous chiral systems may offer a platform for designing more efficient enantioselective interactions, especially by leveraging supramolecular chirality. Supramolecular chiral materials represent a distinct class of intricate and functional materials in chiral chemistry. They often display a higher-level chirality beyond the molecular level chirality of their building blocks.[12] Double-stranded DNAs often consist of chiral building blocks, and display a higher-level chirality beyond the molecular level chirality of their units.[12,13] Thus, pathways for synthetically achieving supramolecular chirality can provide a heterogeneous platform for enantioselective recognition. Fc-derivatives have resulted in higher level chirality,[14] but the study of electrochemically mediated applications for sensing and recognition remains limited.

Here, we report on the synthesis of chiral redox-metallopolymers that possess chirality at a polymer level, induced from a chiral synthesized Fc monomer. We imparted chirality onto redox-metallopolymers through the creation of chiral-Fc-based building blocks, inspired by the well-known Ugi's amine (*N*,*N*-dimethyl-1-ferrocenylethylamine). The corresponding polymer of these chiral redox receptors not only facilitated the fabrication of chiral electrodes by simple deposition on a current collector but also enabled hierarchical chirality, which resulted in the enhancement of their chiral resolution. The chiral Fc units

J. Jeon, J. Elbert, C.-H. Chung, J. Chae, X. Su
Department of Chemical and Biomolecular Engineering
University of Illinois Urbana-Champaign
Urbana, IL 61801, USA
E-mail: x2su@illinois.edu

The ORCID identification number(s) for the author(s) of this article can be found under https://doi.org/10.1002/adfm.202301545.

DOI: 10.1002/adfm.202301545

in our redox-metallopolymers allowed potential-shift-based investigation on enantioselective recognition toward a wide range of chiral amino acids and carboxylates. The enantioselective potential shift of the chiral metallopolymer electrodes could determine enantiomeric excess (%ee) of tryptophan in a range of 0–100%ee L-tryptophan. Our current work seeks to provide a versatile approach for the creation of enantioselective materials, and to demonstrate proof-of-concept of their use in potential-based enantioselective electrochemical sensing toward a wide range of chiral molecules.

2. Results and Discussion

2.1. Design, Synthesis, and Characterization

Here, we design and synthesize two chiral redox-metallopolymers containing an amide (poly-1) or tertiary amine group (poly-2) in the position of the amine of Ugi's amine (**Figure 1**a; see Supporting Information for synthesis details including the yields). The building block of the two chiral redox-metallopolymers was inspired by Ugi's amine (**Figure 2**g), a commercially available Fc derivative with a tertiary amine, methyl group, and cyclopentadienyl rings of Fc around the chiral center. These functional groups can provide various donor-acceptor type interactions for enantioselective recognition. The enantioselective recognition of Ugi's amine was evaluated by measuring its half potential shift ($\Delta E_{1/2}$) upon the addition of ten equivalent tryptophan enantiomers. The opposite affinity of Ugi's amine enantiomers toward the enantiomers was observed as the half potential of (*S*)– and (*R*)-Ugi's amine shifted –77 and –67 mV with L-tryptophan, and –62 and –90 mV with D-tryptophan, respectively (Figure S1, Supporting Information).

For the synthesis of *N*-(1-ferrocenylethyl) methacrylamide ((*S*)– and (*R*)–1), the racemic 1-ferrocenyl-ethylamine was prepared by reductive amination with ammonia and the enantiomers were separated by diastereomeric crystallization with (+)-tartaric acid yielding 96.4%ee (*R*) and (–)–tartaric acid 93.4%ee (*S*) according to high-pressure liquid chromatography (HPLC; Figure S2a, Supporting Information). Consecutively, the amide monomers (*S*)– and (*R*)–1 were prepared by reaction of the corresponding amines with methacryloyl chloride. For 2-((1-ferrocenylethyl)(methyl)amino) ethyl methacrylate ((*S*)– and (*R*)–2), the racemic *N*-methyl-1-ferrocenyl-ethylamine was prepared by reductive amination of acetylferrocene with methylamine and the enantiomers separated by the same crystallization method yielding 96.1%ee (*S*) and 94.7%ee (*R*) (Figure S2b, Supporting Information), followed by the addition of 2-bromoethyl methacrylate to prepare (*S*)– and (*R*)–2. Single-crystal X-ray diffraction revealed the absolute chirality of (*S*)–1 and (*S*)-*N*-methyl-1-ferrocenyl-ethylamine (Tables S11–S24, Supporting Information). NMR, mass spectrometry, and CHN elemental analysis were used to confirm the molecular structures of the products in each step (Figures S3–S20 and Table S1–S6, Supporting Information). (*S*) –1, (*R*)–1, (*S*)–2, and (*R*)–2 were polymerized by free radical polymerization into poly-(*S*)–1 (M_w = 8650), poly-(*R*)–1 (M_w = 26 400), poly-(*S*)–2 (M_w = 11 400), and poly-(*R*)–2 (M_w = 20 800), and ^{1}H NMR and GPC confirmed their structures and molecular weights (Figures S21–S28, Supporting Information). The CD spectra revealed the opposite chirality of the monomers and polymers for both 1 and 2 (Figure 1b–c; Figure S29 (Supporting Information) for the monomers). The Cotton effects observed in the two absorption spectra of π–π^* (250 nm) and *d*–*d* (450 nm) regions (UV–vis in Figure S30, Supporting Information) were attributed mainly to the Fc located right next to the chiral center.

Chiral redox electrodes were fabricated by drop-casting a polymer solution in chloroform on a glassy carbon electrode (GCE). The concentration of the polymers was varied to find the range of an optimal concentration that can circumvent high charge-transfer and diffusion resistance of excess polymer film deposition and was set to 1 mg mL^{-1} for poly-(*S*/*R*)–1 and 1.19 mg mL^{-1} for poly-(*S*/*R*)–2 (Figure S32, Supporting Information). The film thickness of poly-(*S*)–1 was 62 nm near the edge of a glassy carbon substrate and 170 nm at the center based on surface profilometry and 3D laser scanning confocal

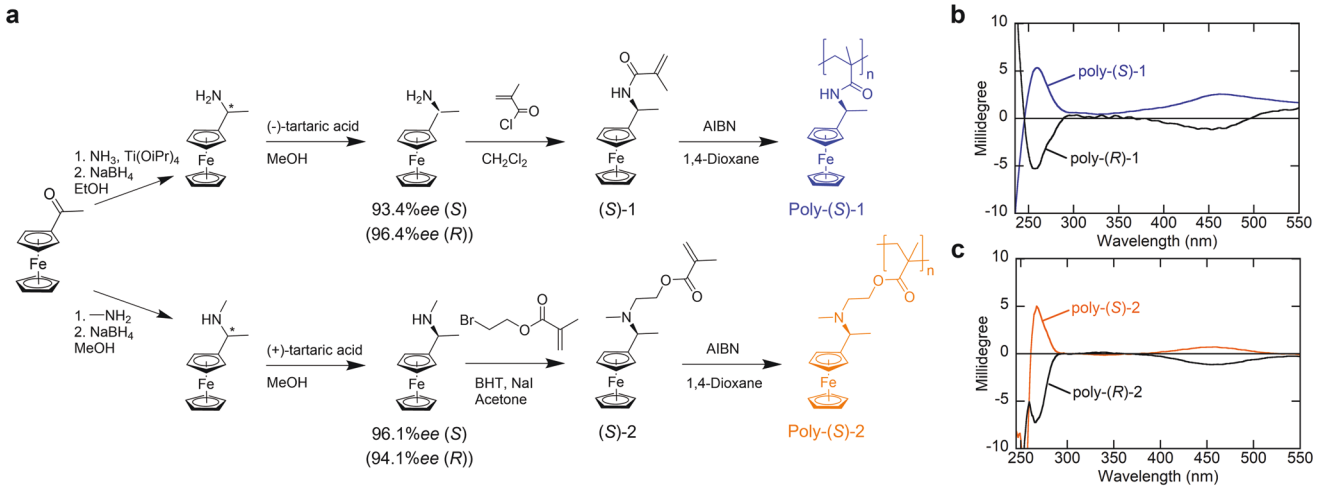

Figure 1. a) Synthesis scheme of poly-(*S*)–1 and poly-(*S*)–2. Reaction conditions are specified in Supporting Information. b,c) Circular dichroism (CD) of 1 mg mL^{-1} poly-(*S*), (*R*)-1 (b) and 1.19 mg mL^{-1} poly-(*S*), (*R*)–2 (c) in tetrahydrofuran (THF).

microscope (Figure S34, Supporting Information). The linear relationship between the peak current and the square root of the voltammetry scan rate described the redox reaction of the polymer film was diffusion-controlled (Figure S35, Supporting Information). The incubation time in an analyte solution was set to 8 min under stirring to reach equilibrium in the analyte binding process (Figure S33, Supporting Information).

2.2. Mechanism for Chiral Redox-Metallopolymer Interaction with Target Enantiomers

Within the current work, redox peak potential shift of the Fc moiety upon complexation with chiral molecules was utilized as means to probe enantioselective interaction. Previously in electrochemical enantioselective recognition, Fc derivatives have been used as an electron-transport mediator and binder without participating in the recognition of an analyte.[10] Peak potential shifts of a host or guest chiral molecule can sense enantioselective interactions and therefore have been used in potential-dependent enantioselective recognitions.[11,15] The illustrative scheme in Figure 2a provides the pathways for possible electrochemical and non-electrochemical binding of the chiral Fc units with L-enantiomer. Square wave voltammetry (SWV) of (*S*)–1, poly-(*S*)–1, (*S*)–2, and poly-(*S*)–2 deposited on GCE demonstrated that the redox reaction occurred at the half potential of 272, 369, 412, and 419 mV versus Ag/AgCl, respectively (Figure 2b,c). The half potential of poly-(*S*)–2 was 50 mV higher than poly-(*S*)–1 due to its tertiary amine that is more electron-withdrawing for the Fc than the amide of poly-(*S*)–1. The high peak currents of the polymers (630 and 420 µA with poly-(*S*)–1 and poly-(*S*)–2) compared to those of the monomers (130 and 160 µA with (*S*)–1 and (*S*)–2) were attributed to their porous structure (SEM in Figure S31, Supporting Information). A Job plot of (*S*)–1 in a homogeneous acetonitrile (MeCN) solution obtained by NMR revealed the 1:1 binding between the chiral Fc unit and chiral analytes (*N*-(*tert*-butoxycarbonyl)-proline (Boc-proline), naproxen, and *N*-(*tert*-butoxycarbonyl)-tryptophan

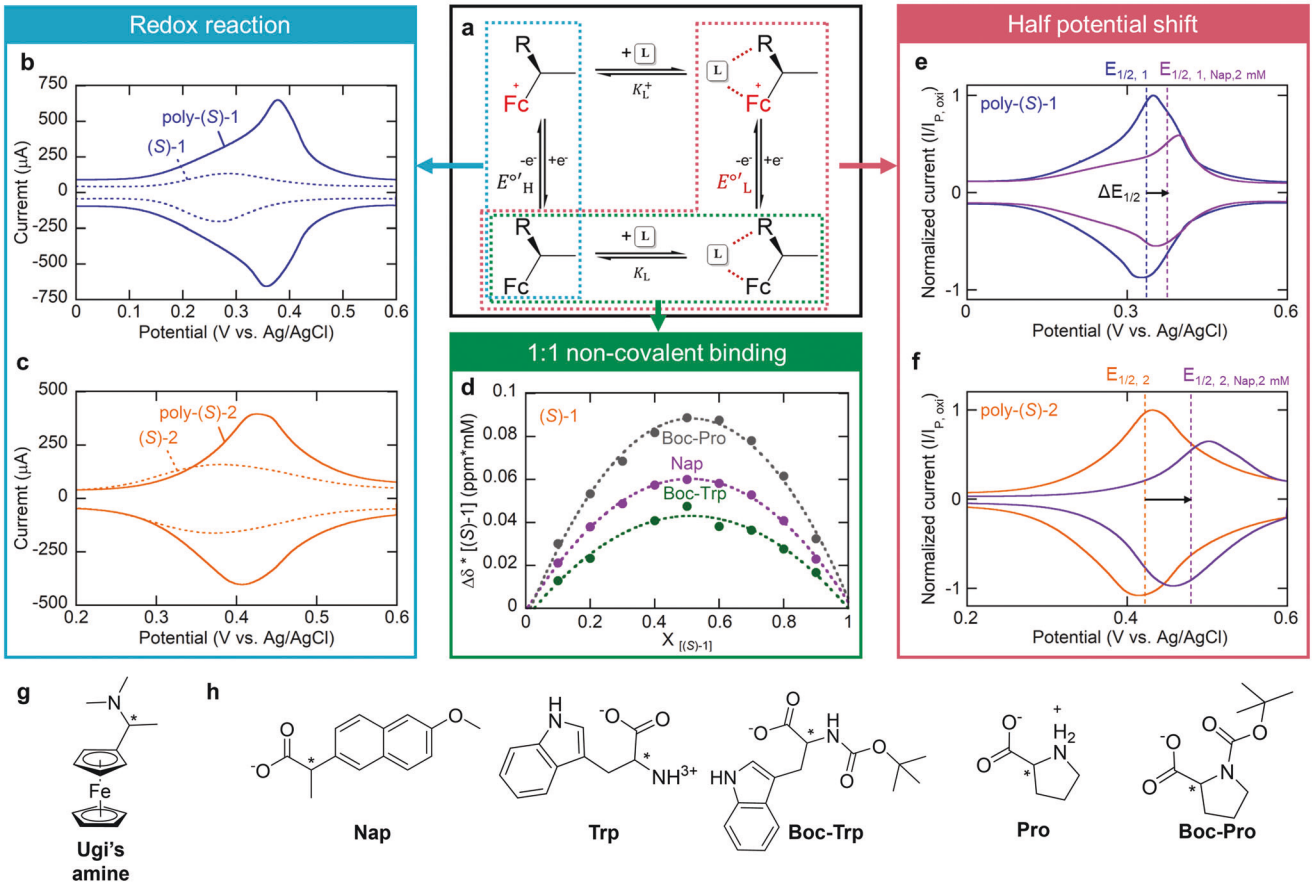

Figure 2. a) Electrochemical square scheme based on chiral Fc molecule binding to L enantiomer, forming two distinct electroactive species. b,c) SWV of the monomer and polymer thin film on GCE in 1× PBS (Phosphate buffer saline) at pH 6.5 (10 mM phosphate buffer in 137 mM sodium chloride, 2.7 mM potassium chloride, and 1.76 mM potassium phosphate; pH was adjusted by HCl); b) (*S*)–1 and poly-(*S*)–1 and c) (*S*)–2 and poly-(*S*)–2. d) Job plot of (*S*)–1 with deprotonated *N*-(*tert*-Butoxycarbonyl)-proline (Boc-Pro), Naproxen (Nap), and *N*-(*tert*-Butoxycarbonyl)-tryptophan (Boc-Trp) obtained from nuclear magnetic resonance (NMR) with 5 mM of the total concentration of (*S*)–1 and the analytes in CD_3CN. e,f) SWV before and after binding with naproxen in 2 mM naproxen 1× PBS, showing the half potential shift ($\Delta E_{1/2}$) of poly-(*S*)–1 (e) and poly-(*S*)–2 (f). g) Chemical structure of Ugi's amine. h) Chemical structures of chiral analytes used in this study. (from left to right) Naproxen (Nap), tryptophan (Trp), Boc-tryptophan (Boc-Trp), proline (Pro), and Boc-proline (Boc-Pro).

(Boc-tryptophan) (Figure 2d). The chemical structures of the analytes used in this study are listed in Figure 2h.

Figure 2e,f shows the half potential shift ($\Delta E_{1/2}$)of poly-(*S*)–1 and poly-(*S*)–2 in the presence of 2 mM (*S*)-naproxen in phosphate buffer saline at pH 6.5 (1× PBS; 10 mM phosphate buffer in 137 mM sodium chloride (NaCl), 2.7 mM potassium chloride (KCl), and 1.76 mM potassium phosphate). The half potential shift of poly-(*S*)–2 (56 mV) was 1.7 times higher than that of poly-(*S*)–1 (33 mV) likely because the protonated amine led to a stronger electrostatic interaction with the anionic naproxen ($K_{Nap,2}>K_{Nap,1}$). The equations of the half potential shift ($\Delta E_{1/2}$) and the half potential shift difference between enantiomers ($|\Delta\Delta E_{1/2}|$) and their relationship to the binding equilibrium constant can be found in Supporting Information. The peak current after the analyte binding decreased by 40%, due to the slower electron transfer of the Fc in the complex than the free Fc. The current decrease of an Fc receptor upon an analyte binding was also previously reported.[16]

2.3. Supramolecular Chirality within the Redox-Polymers and Enhancement in Enantioselective Recognition

2D NMR and solid-state CD of poly-(*S*)–1 and poly-(*S*)–2 revealed their supramolecular chirality induced by the point chirality in their monomer units, which enhanced the enantioselective recognition of the polymers compared to their monomers. The intensities of CD spectra of the monomers and polymers with the same chirality had no noticeable difference in solution (i.e., THF and chloroform), indicating that their optical activity was derived from the point chirality (Figure S29, Supporting Information). However, an intramolecular interaction between the Fc and the backbone of both polymers was detected based on Nuclear Overhauser Effect Spectroscopy (2D NOESY) NMR. Poly-(*S*)–1 presented cross-peaks of protons in the Fc (*c*) with protons in CH_2 (*d*) and CH_3 (*f*) in the backbone, while poly-(*S*)–2 also showed cross-peaks of protons in the Fc (*a*) with protons in CH_2 (*f*) and CH_3 (*h*) in the backbone (**Figure 3**a,b).

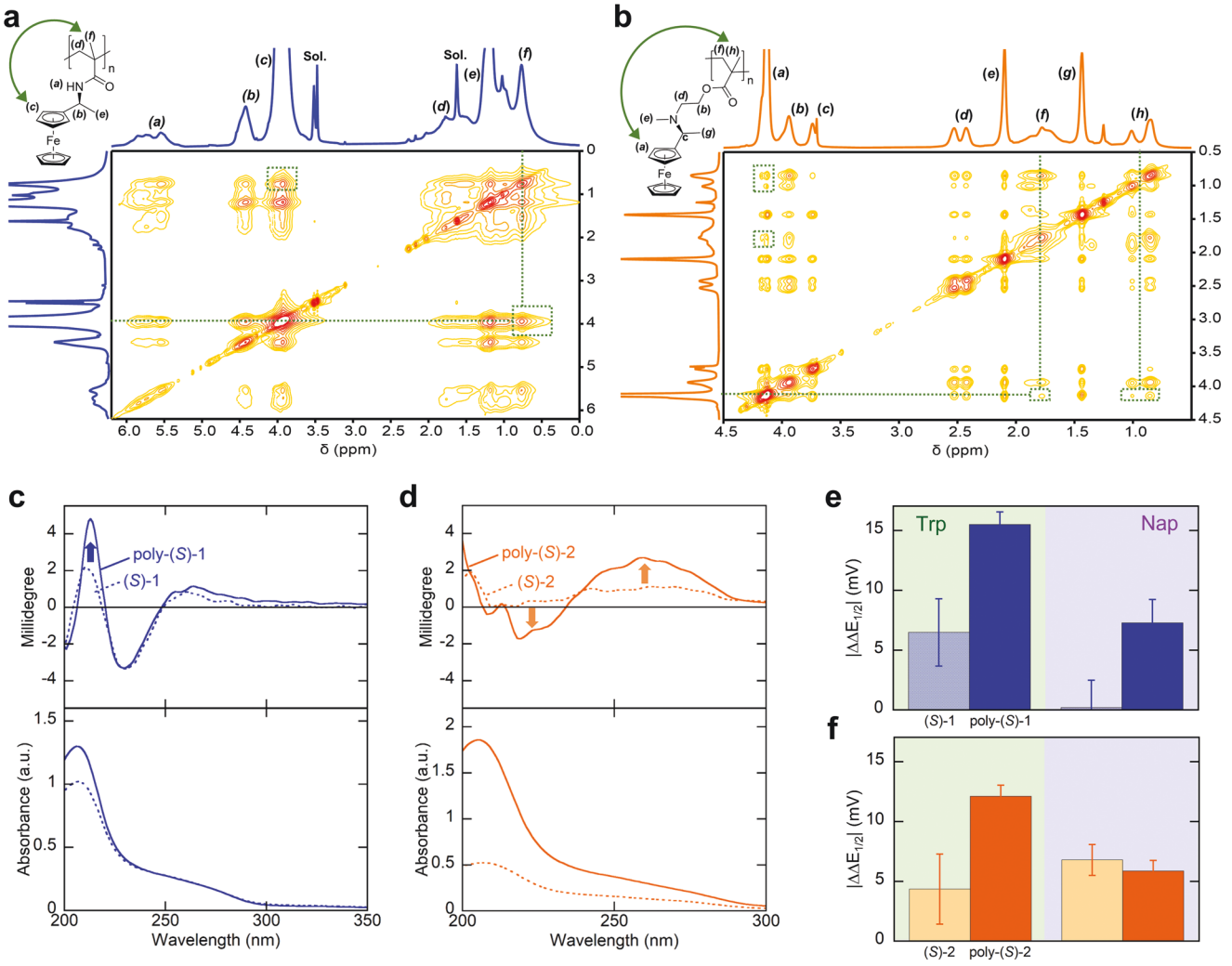

Figure 3. a,b) 2D NOESY spectra of poly-(*S*)–1 (a) and poly-(*S*)–2 (b) in $CDCl_3$ at 500 MHz (12 scans with 300 ms mixing and 2 s delay). Peaks labed as Sol. are solvent peaks. c,d) Solid-state CD (top) and UV absorption (bottom) spectra of (*S*)–1, poly-(*S*)–1 (c), (*S*)–2 and poly-(*S*)–2 (d). The monomers are in dotted lines and the polymers in plain lines. e,f) Half potential difference of (*S*)-1, poly-(S)-1 (e), (S)-2, and poly-(S)-2 (f) in 30 mM enantiopure tryptophan (Trp) and 2 mM enantiopure naproxen (Nap) 1× PBS at pH 6.5.

In contrast, the Fc moiety of the monomers had cross-peaks only with neighboring protons within two carbon chains; the intramolecular interaction was not shown in the 2D NOESY of the corresponding monomers (Figures S38 and S39, Supporting Information).

The solid-state CD and UV–Vis spectra of the polymers and monomers deposited on a quartz substrate showed an intensity increase in both polymers owing to the induced supramolecular chirality (Figure 3c,d). The chirality transfer from the monomer building block to a longer scale in the backbone was attributed to the intramolecular interaction between the Fc and the alkyl group in the backbone of the polymers and the steric hindrance of the Fc leading to the rigidity of the polymers. A bulky Fc closely located to a backbone or a reactive site is reported to exert the steric hindrance giving stiffness to a macromolecule or a decrease in reactivity.[17] Powder XRD of poly-(*S*)–1 and poly-(*S*)–2 gave the *d*-spacing value of 5.76 and 5.79 Å, which indicated a constant distance between neighboring Fc's in the polymers (Figure S40 and Table S8, Supporting Information).

We then compared the half-potential shift difference ($|\Delta\Delta E_{1/2}|$) of poly-(*S*)–1, poly-(*S*)–2, and their corresponding monomers with tryptophan or naproxen. The enantioselective resolution of the polymers increased compared to that of their monomers (Figure 3e,f). With 30 mM tryptophan, poly-(*S*)–1 and poly-(*S*)–2 showed $|\Delta\Delta E_{1/2}|$ of 15.5 and 12.1 mV that were noticeably higher than those of the corresponding monomers (6.5 and 4.4 mV, respectively). With 2 mM naproxen, poly-(*S*)–1 had 7.3 mV of $|\Delta\Delta E_{1/2}|$ while (*S*)–1 showed a negligible $\Delta\Delta E_{1/2}$ (0.2 mV), implying that the size of a binding pocket controlled by the induced supramolecular chirality played a key role to the selectivity. However, poly-(*S*)–2 and (*S*)–2 had a similar selectivity toward naproxen enantiomers (6.8 and 5.9 mV) because the larger pocket from the long alkyl chain between the Fc and the backbone of poly-(*S*)–2 gave less conformational constraint than that of poly-(*S*)–1. Powder XRD of (*S*)–1 showed crystallinity that was attributed to the hydrogen bonding (HB) intermolecular interaction between the amide groups of (*S*)-1 according to ATR-IR (Figures S40 and S41, Supporting Information), which may hamper the enantioselective recognition of the (*S*)-1 electrode. The discrepancy between the half potentials of (*S*)-1 (270 mV) and poly-(*S*)-1 (370 mV) in Figure 2b also explained the less electron-withdrawing property of the amide of (*S*)-1 because of the HB the amide participated. In summary, the supramolecular chirality of the chiral redox-metallopolymers was observed by the solid-state dichroism and this supramolecular chirality could be a primary factor leading to the enhancement in their enantioselective resolution. The conformational constraints originated from the size of the binding pocket formed by the intramolecular interactions of the polymers (Figure 3a,b) and intermolecular interaction between the monomers could further affect the enantioselective resolution difference between the polymers and their monomers.

2.4. Enantioselective Potential Shift of the Chiral Redox-metallopolymers with Tryptophan

We investigated the redox-mediated enantioselective interaction of the chiral redox-metallopolymers and their corresponding monomers with tryptophan (**Figure 4**a–d). The half potential shift of both poly-(*S*)–1 and poly-(*S*)-2 was higher with D-tryptophan (13.5 and 8.4 mV) than the opposite enantiomer, L-tryptophan (7.6 and 5.4 mV), while the half potential of poly-(*R*)–1 and poly-(*R*)–2 shifted more with L-tryptophan (15.8 and 4.2 mV) than with D-tryptophan (9.7 and 2.7 mV), proving the enantioselective interaction of both redox-metallopolymers (Figure 4a,c). The asymmetry between the potential shifts of (*S*) and (*R*) was attributed to the different enantiopurity of the monomers as (*R*)–1 (96.4%ee) and (*S*)-2 (96.1%ee) had higher enantiopurity than (*S*)–1 (93.4%ee) and (*R*)–2 (94.1%ee), respectively. As a result, poly-(*R*)–1 and poly-(*S*)–2 had the higher shift difference ($|\Delta\Delta E_{1/2}|$) (6.1 and 3 mV) than poly-(*S*)–1 and poly-(*R*)–2 (5.9 and 1.5 mV), respectively. The monomer-coated electrodes were also fabricated and tested with the same method and parameters as the polymer electrodes, showing the same potential shift trend toward the tryptophan enantiomers as the polymer-coated electrodes (Figure S36 and S37, Supporting Information). For the comparison between the enantioselective recognition of the amide- and amine-functionalized polymers, their (*S*) forms and corresponding monomers were used in the rest of the study.

Next, the nature of the supporting electrolytes and ionic strength were varied to study their effect on the half potential shift of poly-(*S*)–1 and poly-(*S*)–2 (Figure 4e,f). In addition to $NaClO_4$, 1× PBS at pH 6.5 was chosen to investigate the applicability of our chiral redox polymers in biologically-relevant model mixtures.[10a,b,16,18] In 150 mM $NaClO_4$, the change of the half potential shift ($\Delta E_{1/2}$) and the half potential shift difference ($|\Delta\Delta E_{1/2}|$) of both polymers was marginal within 2.6 mV compared to the values in 20 mM $NaClO_4$. The marginal half potential change was ascribed to the stable ion-paring between a perchlorate anion and a Fc^+. The stable ion-paring between a perchlorate anion and a Fc^+ has been reported.[19]

In 20 mM PBS and 1× PBS, both the half potential shift and the half potential shift difference of the polymers were higher than in the $NaClO_4$ media. Especially, the half potential shift difference in 1× PBS was 4.7 times higher for poly-(*S*)–1 (15.5 mV) and 2.8 times higher for poly-(*S*)–2 (10.8 mV) than in 150 mM $NaClO_4$ (3.3 and 3.9 mV). Given that both electrolytes have similar ionic strength (150 mM for $NaClO_4$, 163 mM for 1× PBS), this shift difference was attributed to the difference of the competing anions, ClO_4^- and Cl^-, making the PBS biological medium suitable for the potential use of the chiral electrodes in sensing. Furthermore, the increase in the half potential shift difference in 1× PBS compared to 20 mM PBS (8.2 mV for poly-(*S*)-1 and 10.6 mV for poly-(*S*)–2) explains that the film swelling helped the enantioselective interaction of the polymers in the PBS medium.

Lastly, an electrolyte without phosphate showed a decrease in the half potential shift difference of poly-(*S*)–1 by 2.5 mV. In contrast, the half potential shift difference of poly-(*S*)–2 increased by 4.8 mV, owing to the absence of the phosphate that can electrostatically bind to the amine of poly-(*S*)–2. The binding between phosphate and amine, which has been previously studied in literature,[20] could potentially hamper the enantioselective binding between tryptophan and the monomer unit. There was no effect of pH on the potential shifts as the pH values of the electrolytes were close to each other between 6.1 and 6.5 and showed no significant change after the experiment (Table S7, Supporting Information).

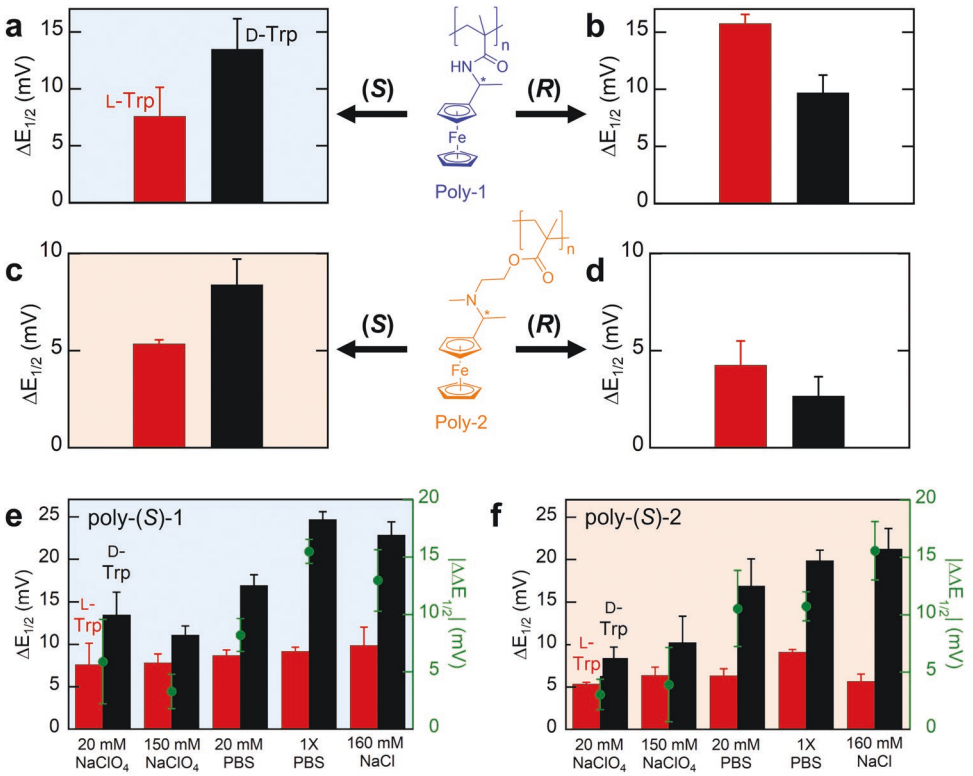

Figure 4. a–d) Enantioselective half potential shift ($\Delta E_{1/2}$) of the chiral redox-metallopolymers with 30 mM L-tryptophan (L-Trp; red bars) and D-tryptophan (D-Trp; black bars) in 20 mM $NaClO_4$; a) Poly-(*S*)-1, b) Poly-(*R*)-1, c) Poly-(*S*)-2, and d) Poly-(*R*)-2. e,f) Half potential shift ($\Delta E_{1/2}$) and half potential shift difference ($\Delta\Delta E_{1/2}$) of poly-(*S*)–1 (e) and poly-(*S*)–2 (f) with 30 mM L- and D-Trp in different electrolytes. 20 mM PBS was diluted from 1× PBS and 160 mM NaCl contained 160 mM NaCl and 3 mM KCl to have the same ionic strength with 1× PBS.

2.5. Analyte-Concentration-Dependent Potential Shift of the Chiral Redox-Metallopolymers

The half potential shift of poly-(*S*)–1 and poly-(*S*)–2 was measured in the presence of varying concentrations of tryptophan or naproxen enantiomers, to evaluate the enantioselective recognition of each chiral redox-metallopolymers against the target analytes. The concentration range was 0.02–2 mM for naproxen and 1–30 mM for tryptophan based on the solubility of each analyte in 1× PBS and potential resolution of the SWV method (0.1 mV). The potential window of SWV was set to 0.0–0.6 V to avoid the interference on the polymer potential shift by the redox activity of tryptophan and naproxen which of the redox potential is above the window (Figure S42, Supporting Information).

Both polymers showed measurable enantioselective recognition toward naproxen as well as tryptophan (**Figure 5**). Poly-(*S*)–1 had a higher potential shift difference than poly-(*S*)–2 over the entire concentration range (Figure 5a,c). The best fitting for $\Delta E_{1/2}$ of the polymers with tryptophan was found with Type 1 Langmuir isotherm, and the adsorption equilibrium constants (K) and maximum half potential shifts ($\Delta E_{1/2,\,m}$) were calculated based on the fittings (Tables S9 and S10, and Figure S43, Supporting Information). For D-tryptophan, both $\Delta E_{1/2,\,m}$ and K_D of poly-(*S*)–1 (27.4 mV and 0.2264 L $mmol^{-1}$) were higher than those of poly-(*S*)–2 (23.64 mV and 0.1198 L $mmol^{-1}$) because COO^- and NH_3^+ of tryptophan could coordinatively form HBs with the amide moieties in poly-(*S*)–1. A similar dimerization between two amides by forming two HBs was also reported in the literature.[21] In contrast, poly-(*S*)–2 can form only one electrostatic interaction between COO^- and the amine of poly-(*S*)–2. For L-tryptophan, one of the HBs with poly-(*S*)–1 was sterically hindered, leading to its low K_L (0.1465 L $mmol^{-1}$) whereas poly-(*S*)–2 had a higher K_L (0.2504 L $mmol^{-1}$) owing to the stronger electrostatic interaction. The Gibbs free energy changes of the adsorption were also calculated based on the equilibrium constants K_L and K_D (Table S9, Supporting Information). $\Delta\Delta G$ of poly-(*S*)–1 and poly-(*S*)–2 were 1.07 and 1.82 kJ mol^{-1}, respectively, which are in the same order of magnitude with π–π interaction, dipole–dipole, and hydrogen bonding.[22] In short, the enantioselectivity toward tryptophan was higher with poly-(*S*)–1 than poly-(*S*)–2 because of the stereospecific interaction by the amide of poly-(*S*)–1.

With 2 mM naproxen, $|\Delta\Delta E_{1/2}|$ was 7.3 and 5.9 mV for poly-(*S*)–1 and poly-(*S*)–2, respectively, with (*S*)-naproxen giving higher peak shifts than (*R*)-naproxen for both polymers (Figure 5b,d). The higher potential shift difference of poly-(*S*)–1 than poly-(*S*)–2 was presumably due to the π–π interaction of the Fc and naphthyl group balanced by the HB between $-COO^-$ and the amide. On the other hand, the electrostatic interaction of poly-(*S*)–2 could likely outweigh other interactions and impeded a stereospecific binding despite higher K_{Nap} than that of poly-(*S*)–1. In summary, poly-(*S*)-1 had the higher $|\Delta\Delta E_{1/2}|$ with the tested analytes than poly-(*S*)-2 although

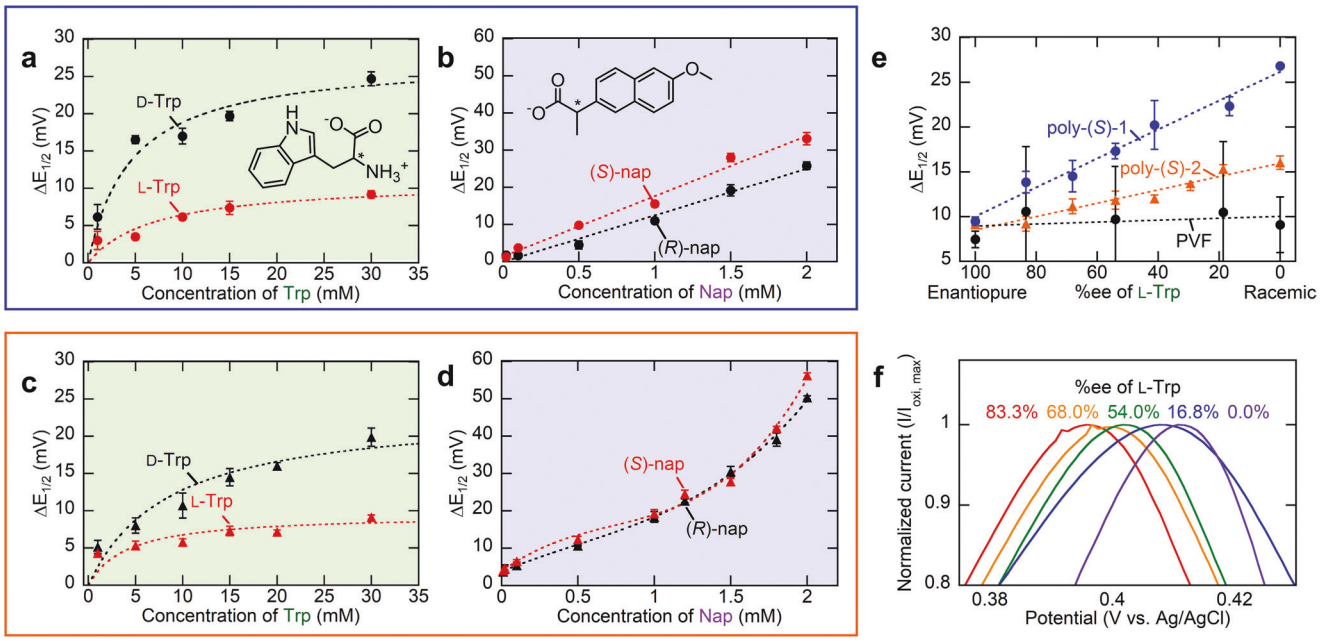

Figure 5. Half potential shift ($\Delta E_{1/2}$) of a,b) poly-(*S*)–1 and c,d) poly-(*S*)-2 in 1–30 mM of L- and D-tryptophan (Trp), 0.02-2 mM of (*S*)- and (*R*)-naproxen (Nap) enantiomers. e) Half potential shift of poly-(*S*)–1 (blue), poly-(*S*)–2 (orange), and PVF (black) in 30 mM tryptophan in the range between enantiopure L-Trp and racemic Trp. The chiral polymers showed linear dependence over this range. f) Oxidation peaks of poly-(*S*)-1 in SWV at various %ee. Both half potential and oxidation potential increased toward the racemic mixture due to the stronger binding with D-Trp than with L-Trp.

poly-(*S*)–2 had the higher $\Delta E_{1/2}$ with the anionic chiral analyte, naproxen.

2.6. Analyte-%ee-Dependent Potential Shift of the Chiral Redox-Metallopolymers

The half potential shift of the polymers with different %ee at a fixed concentration of tryptophan was measured, to evaluate the potential application of the polymers for electrochemical enantioselective sensing (Figure 5e). Importantly, a linear dependence of the half potential shift on %ee was observed for both polymers over a wide range of 0–100%ee L-tryptophan. The slope of the shift ($\Delta E_{1/2}$) of poly-(*S*)–1 (0.162 mV %ee^{-1} with $R^2 = 0.98$) was steeper than poly-(*S*)–2 (0.075 mV %ee^{-1} with $R^2 = 0.95$) over this range owing to the higher enantioselectivity of poly-(*S*)–1 than poly-(*S*)–2. Figure 5f shows oxidation peak potentials of poly-(*S*)–1 at various %ee of L-tryptophan and the potential shift to a higher potential. In contrast, the potential shift of polyvinyl ferrocene (PVF), a polymer with an achiral Fc moiety, stayed the same (0.011 mV %ee^{-1} with $R^2 = 0.12$) over the %ee range (Figure 5e). This result demonstrated the simple insertion of the chirality between the Fc and the vinyl backbone can impart enantioselectivity over an atomically non-chiral backbone, which then can be potentially used as an electrochemical sensor for enantiomers. Future studies are envisioned to focus on enhancing resolution.

Interestingly, the $\Delta E_{1/2}$ of both polymers had little to no change over the range of 0–100%ee D-tryptophan (Figure S44, Supporting Information). The comparison between the experimental and theoretical $\Delta E_{1/2}$ using the calculated adsorption equilibrium constants revealed that the adsorption of L- and D-tryptophan onto the binding sites of the polymers is not entirely competitive. There are possible interactions between L- and D-tryptophan on adjacent sites, or possibly additional tryptophan binding to a polarized tryptophan that is already bound to a binding site. As previously reported in the literature, the tryptophan binding strength differs among L- and L-tryptophan, D- and D-tryptophan, and L- and D-tryptophan because of their zwitterionic property, and L- and D-tryptophan form the most stable binding,[23] thus leading to the higher potential shift of the polymers than with the assumption of the competitive binding between the enantiomers.

2.7. Enantioselective Recognition Mechanism of the Chiral Redox-Metallopolymers

We investigated the effect of the solvent polarity and solution pH, as well as the selectivity mechanism of poly-(*S*)–1 and poly-(*S*)–2 by using a series of representative enantiomers. The magnitude of the half potential shift difference ($|\Delta\Delta E_{1/2}|$) of poly-(*S*)–1 and poly-(*S*)–2 with tryptophan, naproxen, Boc-proline, and proline had a strong correlation with the presence or absence of an aromatic group in an analyte, regardless of its net charge (**Figure 6**a). Tryptophan showed a noticeable potential difference due to its indole group (15.5 and 12.1 mV for poly-(*S*)–1 and poly-(*S*)–2, respectively). Especially, the $|\Delta\Delta E_{1/2}|$ of 2 mM naproxen (7.3 and 5.9 mV for poly-(*S*)–1 and poly-(*S*)–2) was significantly higher than the other analytes (30 mM) due to its naphthyl group, the bulkiest aromatic group among the aromatic groups of the analytes. However, in each 30 mM enantiopure Boc-proline and proline, only poly-(*S*)–1 and Boc-proline showed a shift difference (3.0 mV) (Figure S46, Supporting

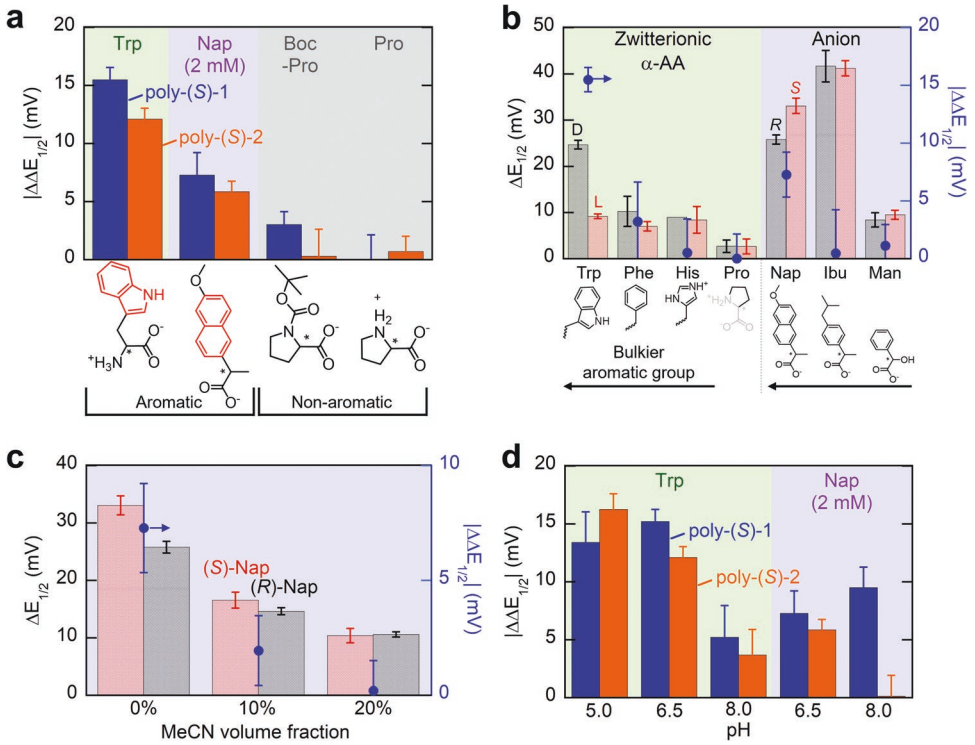

Figure 6. a) Half potential difference of poly-(*S*)–1 (blue) and poly-(*S*)–2 (orange) in enantiopure 30 mM tryptophan (Trp) (green), 2 mM naproxen (Nap) (purple), 30 mM Boc-proline (Boc-Pro), and 30 mM proline (Pro) (gray). b) Half potential shift (on left) and difference (on right) of poly-(*S*)–1 in 30 mM zwitterionic α-AAs (green) and 2 mM anionic carboxylates (purple). Phenylalanine (Phe), histidine (His), ibuprofen (Ibu), and mandelic acid (Man) were additionally used. The chemical structure of the R group of the amino acids and carboxylates were located below the figure. c) Half potential shift and shift difference of poly-(*S*)–1 with 2 mM naproxen in different volume fractions of MeCN in 1× PBS. d) Half potential shift difference of poly-(*S*)–1 and poly-(*S*)–2 with enantiopure 30 mM tryptophan and 2 mM naproxen at pH 5.0, 6.5, and 8.0.

Information). This dependency suggests the importance of the steric effect of an aromatic group and its π–π interaction (π–π) with the Fc of the polymers for the enantioselective recognition. Figure 6b shows the half potential shift of poly-(*S*)–1 with zwitterionic α-amino acids and carboxylates with an aromatic group. An analyte with a bigger aromatic group generally led to a higher $\Delta E_{1/2}$ and $|\Delta\Delta E_{1/2}|$ of poly-(*S*)–1 regardless of the charge of an analyte. Tryptophan showed a higher $|\Delta\Delta E_{1/2}|$ and $\Delta E_{1/2}$ than those of phenylalanine and histidine, whereas proline showed a negligible $\Delta E_{1/2}$ (2.7 mV) and 0 mV of $|\Delta\Delta E_{1/2}|$. Among the carboxylates, naproxen showed the highest $\Delta\Delta E_{1/2}$ (7.3 mV). The selectivity dependency on the size of an aromatic group suggested that a bulkier aromatic group led to more steric hindrance for a stereospecific interaction as well as π–π coordinating with HBs.

We next studied the effect of solvent polarity through the addition of MeCN, and the effect of pH through pH adjustment to investigate the strength change of the involved interactions (i.e., π–π and HB). First, in the solvent polarity experiments, the $|\Delta\Delta E_{1/2}|$ of poly-(*S*)–1 with naproxen dropped from 7.3 to 2.0 mV with 10% MeCN and to 0.2 mV with 20% MeCN (Figure 6c). A less polar and aprotic environment generally leads to an increase in the strength of HB and a decrease in the strength of π–π between an adsorbate and adsorbent.[24] $\Delta E_{1/2}$ also decreased because weaker π–π between the naphthyl group and the Fc resulted in a lower K_{Nap} than in 0% MeCN (Equation S2, Supporting Information). Also, the peak shift of (*S*)–1 and (*S*)–2 dissolved in dry MeCN showed little to no $|\Delta\Delta E_{1/2}|$ (within the confidence limit) for deprotonated naproxen, Boc-proline, and Boc-tryptophan enantiomers at various concentrations due to the strong HB outweighing other interactions (Figure S45, Supporting Information). Hence, it is key to have a subtle balance among the strengths of interactions between a chiral host and guest for high enantioselectivity in redox-mediated electrochemical recognition, in alignment with previous enantioselective recognition studies.[25]

The pH of 1× PBS was varied between 5.0 and 8.0 to adjust the HB strength (Figure 6d). With the same enantiomer affinity toward D-tryptophan, $|\Delta\Delta E_{1/2}|$ of poly-(*S*)–1 dropped both at the acidic and basic pH (13.4 mV at pH 5.0 and 5.2 mV at pH 8.0). The decrease was more significant at the basic pH, where the HB between $-NH_3^+$ of tryptophan and the amide $-CO$ of poly-(*S*)–1 became weaker. This result suggests that the stereospecific interaction accounting for the enantioselectivity of poly-(*S*)–1 was predominantly due to the HB of the $-NH_3^+$ of tryptophan and $-CO$ of poly-(*S*)–1. On the other hand, the selectivity of poly-(*S*)–1 toward naproxen anions did not decrease at pH 8.0, because of the maintained balance between π–π and HB of $-COO^-$ and amide NH, as well as the absence of $-NH_3^+$. The selectivity of poly-(*S*)–2 for both tryptophan and naproxen declined at the higher pH due to the decreasing strength of the electrostatic interaction between $-COO^-$ and $-NH^+$, which was outcompeted by π–π as the pH became basic. Such pH-dependent strength of electrostatic

interaction between $-COO^-$ and $-NH^+$ have been seen in biological macromolecules previously.[24c,26] In sum, our results suggest a balance of interactions depending on the structural motifs of the redox-receptor and target analyte identity, with hydrogen bonding and π–π playing a key role in determining enantioselectivity.

3. Conclusion

In this work, we have designed and synthesized chiral redox-metallopolymers, based on chiral Fc monomers as building blocks, poly-1 with amide-functionalized ferrocene and poly-2 with amine-functionalized ferrocene for heterogeneous enantioselective recognition. The chiral redox-electrodes were investigated for enantioselective potential-shift-based binding towards a range of enantiomers of amino acids and carboxylates. Especially, we found out that the chiral Fc unit not only enabled enantioselective electrochemical sensing, but also induced supramolecular chirality effects observed by CD, and leading to the resulting enhancement of recognition. The chiral redox-polymers presented significantly higher enantioselective recognition toward tryptophan and naproxen, compared to the corresponding redox-monomers. The effect of hydrogen bonding, solvent effects, and structural motifs of the enantiomer analytes are evaluated by electrochemical characterization. Our current work provides a new avenue for the design of chiral redox-metallopolymers and their use in electrochemical potential-based enantioselective sensing toward a range of chiral molecules including amino acids, pharmaceuticals, and organic carboxylates. Future efforts will be directed toward designing inducing controllable supramolecular chirality through a systematic synthetic approach, to achieve even higher enhancement of the enantioselective resolution toward a broader enantiomer scope.

Supporting Information

Supporting Information is available from the Wiley Online Library or from the author.

Acknowledgements

X.S. would like to thank funding from National Science Foundation (NSF) under NSF CBET Grant #1942971. J.J. and X.S. would like to thank Prof. Catherine Murphy for the instrumentation for circular dichroism. J.J. thanks Riccardo Candeago and Shisang Roh for operating the profilometer and helping investigate the recognition function of the polymers. The authors acknowledge the use of instrumentation at NMR Lab, George L. Clark X-Ray Facility (Q-Tof Ultima mass spectrometer purchased in part with a grant from the NSF DBI-0100085), and Microanalysis Laboratory in the School of Chemical Sciences, and in the Materials Research Laboratory Central Research Facilities, University of Illinois, partially supported by NSF (DMR-1720633).

Conflict of Interest

The authors declare no conflict of interest.

Data Availability Statement

The data that support the findings of this study are available from the corresponding author upon reasonable request.

Keywords

chiral metallopolymers, electrochemical chiral sensing, molecular recognition, polymers

Received: February 10, 2023
Revised: March 5, 2023
Published online:

[1] G. A. Hembury, V. V. Borovkov, Y. Inoue, *Chem. Rev.* **2008**, *108*, 1.
[2] a) W. H. Pirkle, T. C. Pochapsky, *Chem. Rev.* **1989**, *89*, 347; b) Y. Liu, W. Xuan, Y. Cui, *Adv. Mater.* **2010**, *22*, 4112.
[3] S. J. Park, I.-S. Hwang, Y. J. Chang, C. E. Song, *J. Am. Chem. Soc.* **2021**, *143*, 2552.
[4] E. Ronchi, S. M. Paradine, E. N. Jacobsen, *J. Am. Chem. Soc.* **2021**, *143*, 7272.
[5] a) Y.-P. Xue, C.-H. Cao, Y.-G. Zheng, *Chem. Soc. Rev.* **2018**, *47*, 1516; b) M. T. Reetz, M. Garcia-Borràs, *J. Am. Chem. Soc.* **2021**, *143*, 14939.
[6] T. Zhu, S. Xu, A. Rahman, E. Dogdibegovic, P. Yang, P. Pageni, M. P. Kabir, X. d. Zhou, C. Tang, *Angew. Chem.* **2018**, *130*, 2412.
[7] a) J.-C. Eloi, D. A. Rider, G. Cambridge, G. R. Whittell, M. A. Winnik, I. Manners, *J. Am. Chem. Soc.* **2011**, *133*, 8903; b) L. Zhang, L. Qin, X. Wang, H. Cao, M. Liu, *Adv. Mater.* **2014**, *26*, 6959.
[8] a) J. Zhang, J. Yan, P. Pageni, Y. Yan, A. Wirth, Y.-P. Chen, Y. Qiao, Q. Wang, A. W. Decho, C. Tang, *Sci. Rep.* **2015**, *5*, 11181; b) K. Zhang, X. Feng, C. Ye, M. A. Hempenius, G. J. Vancso, *J. Am. Chem. Soc.* **2017**, *139*, 10029.
[9] a) X. Su, H. J. Kulik, T. F. Jamison, T. A. Hatton, *Adv. Funct. Mater.* **2016**, *26*, 3394; b) R. Chen, J. Feng, J. Jeon, T. Sheehan, C. Rüttiger, M. Gallei, D. Shukla, X. Su, *Adv. Funct. Mater.* **2021**, *31*, 2009307; c) K. Kim, S. Cotty, J. Elbert, R. Chen, C. H. Hou, X. Su, *Adv. Mater.* **2020**, *32*, 1906877; d) S. Cotty, J. Jeon, J. Elbert, V. S. Jeyaraj, A. V. Mironenko, X. Su, *Sci. Adv.* **2022**, *8*, eade3094.
[10] a) X. Niu, X. Yang, Z. Mo, R. Guo, N. Liu, P. Zhao, Z. Liu, M. Ouyang, *Electrochim. Acta* **2019**, *297*, 650; b) X. Niu, Z. Mo, X. Yang, C. Shuai, N. Liu, R. Guo, *Bioelectrochemistry* **2019**, *128*, 74; c) I. Pandey, S. S. Jha, *Electrochim. Acta* **2015**, *182*, 917; d) Y.-X. Sun, D.-D. Zhang, Y. Sheng, D. Xu, R. Zhang, M. Bradley, *Anal. Methods* **2021**, *13*, 2011; e) G. R. Whittell, M. D. Hager, U. S. Schubert, I. Manners, *Nat. Mater.* **2011**, *10*, 176.
[11] a) G. Mirri, S. D. Bull, P. N. Horton, T. D. James, L. Male, J. H. Tucker, *J. Am. Chem. Soc.* **2010**, *132*, 8903; b) Y. Willener, K. M. Joly, C. J. Moody, J. H. Tucker, *J. Org. Chem.* **2008**, *73*, 1225; c) A. Mulas, Y. Willener, J. Carr-Smith, K. M. Joly, L. Male, C. J. Moody, S. L. Horswell, H. V. Nguyen, J. H. Tucker, *Dalton Trans.* **2015**, *44*, 7268.
[12] a) Y. Sang, M. Liu, *Chem. Sci.* **2022**, *13*, 633; b) J. S. Richardson, *Adv. Protein Chem.* **1981**, *34*, 167; c) J.-S. Wang, G. Wang, X.-Q. Feng, T. Kitamura, Y.-L. Kang, S.-W. Yu, Q.-H. Qin, *Sci. Rep.* **2013**, *3*, 3102.
[13] M. Reggelin, M. Schultz, M. Holbach, *Angew. Chem., Int. Ed.* **2002**, *41*, 1614.
[14] a) Y. Wang, W. Qi, R. Huang, X. Yang, M. Wang, R. Su, Z. He, *J. Am. Chem. Soc.* **2015**, *137*, 7869; b) P. Sun, T. Zhang, H. Luo, J. Dou, W. Bian, Z. Pan, A. Zheng, B. Zhou, *New J. Chem.* **2021**, *45*, 10002.
[15] a) X. Shi, Y. Wang, C. Peng, Z. Zhang, J. Chen, X. Zhou, H. Jiang, *Electrochim. Acta* **2017**, *241*, 386; b) H. Zhou, R. Yu, G. Ran, S. Moussa, Q. Song, J. Mauzeroll, J.-F. Masson, *Sens. Actuators, B* **2020**, *319*, 128315; c) B.-C. Iacob, E. Bodoki, C. Farcau, L. Barbu-Tudoran, R. Oprean, *Electrochim. Acta* **2016**, *217*, 195.

[16] D. Wu, C. Ma, F. Pan, Y. Tao, Y. Kong, *Anal. Chem.* **2021**, *93*, 10160.
[17] a) D. Ge, R. Levicky, *Chem. Commun.* **2010**, *46*, 7190; b) L. Gan, J. Song, S. Guo, D. Jańczewski, C. A. Nijhuis, *Eur. Polym. J.* **2016**, *83*, 517.
[18] L. Guo, Y. Huang, Q. Zhang, C. Chen, D. Guo, Y. Chen, Y. Fu, *J. Electrochem. Soc.* **2014**, *161*, B70.
[19] a) C.-S. Lu, X.-M. Ren, C.-J. Hu, H.-Z. Zhu, Q.-J. Meng, *Chem. Pharm. Bull.* **2001**, *49*, 818; b) G. Valincius, G. Niaura, B. Kazakevičienė, Z. Talaikytė, M. Kažemėkaitė, E. Butkus, V. Razumas, *Langmuir* **2004**, *20*, 6631.
[20] a) S. L. Tobey, E. V. Anslyn, *J. Am. Chem. Soc.* **2003**, *125*, 14807; b) M. A. Hossain, J. A. Liljegren, D. Powell, K. Bowman-James, *Inorg. Chem.* **2004**, *43*, 3751; c) O. Karagollu, M. Gorur, F. Gode, B. Sennik, F. Yilmaz, *Sens. Actuators, B* **2014**, *193*, 788.
[21] A. Johansson, P. Kollman, S. Rothenberg, J. McKelvey, *J. Am. Chem. Soc.* **1974**, *96*, 3794.
[22] J. W. Steed, J. L. Atwood, *Supramolecular Chemistry*, John Wiley & Sons, Hoboken, New Jersey **2022**.
[23] Y. Li, *Master Thesis*, Memorial University of Newfoundland, **2014**.
[24] a) P. A. Sigala, E. A. Ruben, C. W. Liu, P. M. B. Piccoli, E. G. Hohenstein, T. J. Martínez, A. J. Schultz, D. Herschlag, *J. Am. Chem. Soc.* **2015**, *137*, 5730; b) S. Grimme, *Angew. Chem., Int. Ed.* **2008**, *47*, 3430; c) M. S. Cubberley, B. L. Iverson, *J. Am. Chem. Soc.* **2001**, *123*, 7560.
[25] a) M. V. Rekharsky, Y. Inoue, *J. Am. Chem. Soc.* **2002**, *124*, 813; b) L.-E. Guo, Y.-X. Tang, S.-Y. Zhang, Y. Hong, X.-S. Yan, Z. Li, Y.-B. Jiang, *Org. Biomol. Chem.* **2020**, *18*, 4590; c) S. R. Domingos, C. Pérez, N. M. Kreienborg, C. Merten, M. Schnell, *Commun Chem* **2021**, *4*, 32.
[26] a) J. L. Wood, *Biochem. J.* **1974**, *143*, 775; b) A. Kantardjiev, B. Atanasov, *Sequence and Genome Analysis: Methods and Applications*, Zhongming Zhao (*iConcept, 2011*) **2011**.